Cement and Concrete Research 40 (2010) 1023–1033

Contents lists available at ScienceDirect

Cement and Concrete Research

journal homepage: http://ees.elsevier.com/CEMCON/default.asp

Early hydration and setting of oil well cement

Jie Zhang [a], Emily A. Weissinger [a], Sulapha Peethamparan [b], George W. Scherer [a,*]

[a] Dept of Civil and Environmental Engineering, Princeton University, Princeton, NJ 08544, USA
[b] Dept of Civil and Environmental Engineering, Clarkson University, Potsdam, NY 13699, USA

ARTICLE INFO

Article history:
Received 22 December 2009
Accepted 17 March 2010

Keywords:
A. Hydration
A. Kinetics
A. Workability
C. Shrinkage
D. Admixture

ABSTRACT

A broad experimental study has been performed to characterize the early hydration and setting of cement pastes prepared with Class H oil well cement at water-to-cement ratios (w/c) from 0.25 to 0.40, cured at temperatures from 10 to 60 °C, and mixed with chemical additives. Chemical shrinkage during hydration was measured by a newly developed system, degree of hydration was determined by thermogravimetric analysis, and setting time was tested by Vicat and ultrasonic velocity measurements. A Boundary Nucleation and Growth model provides a good fit to the chemical shrinkage data.

Temperature increase and accelerator additions expedite the rate of cement hydration by causing more rapid nucleation of hydration products, leading to earlier setting; conversely, retarder and viscosity modifying agents delay cement nucleation, causing later setting times. Lower w/c paste needs less hydration product to form a percolating solid network (i.e., to reach the initial setting point). However, for the systems evaluated, at a given w/c, the degree of hydration at setting is a constant, regardless of the effects of ambient temperature or the presence of additives.

1. Introduction

In oil well cementing, a cement slurry is pumped through a steel casing to the bottom of the well and then up through the annulus between the casing and the surrounding rock. The two principle functions of the primary cementing process are to restrict fluid movement between formations (e.g., to isolate fluids such as water or gas in one zone from oil in another zone) and to bond and support the casing [1,2]. As cement descends into the well, the slurry is hydrating under elevated temperature, T, and pressure, p. The entire depth of a well is not cemented in a single operation, but even so, pumping can take several hours, and retarders and dispersants are widely employed to prevent premature hardening. The high temperature, high pressure, and the additives involved make oil well cementing a challenging process.

The rate of increase in viscosity is the most important property in the well cementing operation. When the viscosity of the slurry exceeds a few Pa s, it becomes too difficult to pump, so it is essential that this limit not be reached before the cement paste fills the annulus [1]. Setting transforms the paste from a workable plastic slurry into a rigid material. Since setting occurs when the amount of product is sufficient to cause the particles to overlap, forming a continuous solid network, it can be regarded as a percolation process. Knowing the setting time of oil well cement is essential for scheduling the drilling operation. After the cement is pumped into place, the well is left shut for a sufficient time to allow the cement to harden before resuming drilling to a deeper horizon. To avoid damage to the pumping equipment used to place the cement slurry, the cement must remain in a fluid state for several hours while it is pumped into place; to avoid wasting valuable rig time, the cement should set shortly after being placed. Thus, to understand the hydration process and predict the setting time of oil well cement slurries are of considerable economic importance. Some factors that may affect setting time include water-to-cement ratio (w/c), the composition and particle size distribution of cement, presence of additives (mineral and chemical), temperature, and pressure [3]. A low w/c, small cement particles, accelerators, high temperature and high pressure will reduce the setting time [3]. It has been shown that the rate of increase of slurry viscosity over a range of temperature and pressure is described by an activation energy and activation volume [4], so the viscosity can be predicted quantitatively during a variation of T and p.

The American Petroleum Institute (API) has defined various classes of Portland cement, of which Class G and Class H are widely used in well cementing. In this paper, a Class H cement is studied. The specification of Class H cement is typically consistent with sulfate-resisting Portland cements, coarsely ground to 200–260 $m^2\,kg^{-1}$ [3]. The hydration of Class H cement is similar to ordinary Portland cement. Tricalcium silicate ($3CaO\cdot SiO_2$, or C_3S)[1] is the main mineral constituent; it hydrates and hardens rapidly and is largely responsible for initial set and early strength gain. Gypsum in Class H cement is minimized to permit good response to admixtures, so less tricalcium aluminate ($3CaO\cdot Al_2O_3$, or C_3A) is included. Various admixtures are used to modify the physical properties of the slurry, though some have incidental chemical effects

* Corresponding author. Tel.: +1 609 258 5680; fax: +1 609 258 1563.
E-mail address: scherer@princeton.edu (G.W. Scherer).

[1] Cement chemistry notation: C = CaO, S = SiO_2, H = H_2O, A = Al_2O_3, F = Fe_2O_3.

0008-8846/$ – see front matter © 2010 Elsevier Ltd. All rights reserved.
doi:10.1016/j.cemconres.2010.03.014

that are countered by the use of further admixtures. Retarders and dispersants (water reducers) are widely employed, especially in the deeper wells and also to counteract the effects of other admixtures that have incidental accelerating effects. Accelerators, such as $CaCl_2$ are also used. Despite the importance of controlling early hydration and setting of oil well cement exposed to high temperature and pressure and rate-controlling chemical additives, the fundamental mechanisms underlying the reaction process are not well understood, and there is no single theory that can explain all of the major observations associated with the early hydration of oil well cements.

There are a variety of experimental ways to study the early hydration kinetics of cement. Some methods follow the rate of the reaction continuously, while others test the physical or chemical properties of the paste at intervals in time [5,6]. Computational and mathematical models have been established to explain cement hydration and predict materials properties [7–11]. In oil well cementing, Jupe et al. [12,13] used an in-situ synchrotron X-ray diffraction to examine the real time hydration of Class H cement slurries at high temperatures and high pressures. In this study, the early hydration of Class H cement and its setting are studied by multiple techniques. A chemical shrinkage measurement is used to quantify the rate of hydration of cement paste at various temperatures, w/c, and under the influence of several additives. During the chemical shrinkage experiments, samples were taken from the same mixing batch and had their hydration arrested at the initial setting time determined using the Vicat test. An ultrasonic transmission measurement was also compared with the Vicat test. The degree of cement hydration at the setting time was analyzed by thermogravimetric analysis (TGA). To obtain sufficient time resolution, a freeze-drying procedure was used to stop the hydration instantaneously at the setting time for TGA measurement. A mathematical nucleation and growth model developed by Avrami [14–16] and Cahn [17,18] was applied to the chemical shrinkage data to describe the growth and nucleation characteristics of each sample.

2. Materials and methods

2.1. Experimental materials

The Class H oil well cement used in this study was manufactured by Lafarge and provided by Halliburton. Upon delivery, the cement was packed separately in sealed plastic bags and sealed in metal cans with 1 kg of cement in each container. Its mineral composition, analyzed by X-ray diffraction (XRD), is shown in Table 1. The surface area of the cement was measured by the BET method using nitrogen as the adsorptive in a Micromeritics Autosorb 2010.

This study focused on the effects of temperature ($T = 10$, 25, 40 and 60 °C), water-to-cement weight ratio (w/c = 0.25, 0.35 and 0.40), and additives (maltodextrin (MD), calcium chloride ($CaCl_2$), hydroxyethylcellulose (HEC), and diutan (DT)) on the hydration kinetics. Given the low C_3A content of the cement and the restriction to $T \leq 60$ °C, the hydration products are expected to be similar to those found at ambient temperature. New phases occur at higher temperatures [3,19]. Maltodextrin is a white hygroscopic powdered carbohydrate derived from maize starch that retards the thickening of the cement slurry without delaying compressive strength development [20]. The MD used in this study (FDP-C817-05, undiluted) was provided by Halliburton Energy Services. In addition to acceleration of the initial set [3], $CaCl_2$ has several other effects: it increases the rate of heat generation during the first hours after slurry mixing; it increases the yield point of a cement slurry (plastic viscosity); and it significantly increases the rate of compressive strength development during the first few days after placement [2]. The $CaCl_2$ used in this study was obtained from EMD Chemical Inc. HEC is a "fluid-loss control agent" [21] that inhibits escape of the aqueous phase of the slurry into the formation (i.e., the rock surrounding the well) by reducing the permeability of the filter cake of cement solids and increasing the viscosity of the aqueous phase. HEC is the most common cellulosic fluid-loss control agent. One of the disadvantages of the cellulosic fluid-loss additives is that, at temperature less than 65 °C, this type of additive is an efficient retarder [2]. The HEC used in this study was FWCA™ cement additive supplied by Halliburton Energy Services. Diutan is a high molecular weight, microbial polysaccharide produced by aerobic fermentation that is used as a viscosity modifying agent in cement slurries [22]; it is effective for controlling bleeding by the formation of a viscous gel. Several researchers have used both water reducing agents (e.g., superplasticizers) and viscosity modifying agents to improve the rheological properties and the performance of cement paste. In this study, no superplasticizer was used with DT. There were two batches of DT used in this study, which we distinguished as DT1 and DT2. They were in the form of Geovis XT and were manufactured by Kelco Oil Field Group and provided by Halliburton. HEC and DT are both found to mildly retard the hydration.

Table 1
Compound component and BET surface area of Class H cement (wt%).

Component	C_3S	C_2S	C_3A	C_4AF	Gypsum	BET Surface area (m^2/g)
Class H	63.94	15.84	0.57	11.33	1.8	1.00 ± 0.0075

A standardized procedure was used for mixing the cement paste for all the experiments in this study. This procedure was developed by PCA [23], and used by Ferraris [24]. A seven-speed Waring laboratory blender with a 1.25 L borosilicate glass jar was used. This blender has a speed controller which provides seven blade speeds from 3500 to 21,000 rpm that can be held constant regardless of the load. The mixing water, blender, and all the paste containers were preheated (or precooled) to the temperature required prior to mixing. Right before mixing, the inside of the glass jar was moistened using a wet paper towel. Next, the deionized water and any admixture were poured into the container. While the mixer blades rotate at a speed of about 3500 rpm the cement is introduced within 30 s. An appropriate amount of mixture (around 550 g in this study) was used to make sure that it was not too little to cover the blades, or too much to be mixed thoroughly. After the transfer, mixing continued at 3500 rpm for another 30 s. Next, the speed of the blades was increased to about 9300 rpm for an additional 30 s. At this point, the mixer was stopped and the paste was scraped down from the walls of the jar. After 2.5 min of resting, the blender was turned on again at a speed of 9300 rpm for 30 s. The cement paste that was prepared for measurement of chemical shrinkage was mixed using deionized water that was de-aired by boiling and then cooled to room temperature before mixing. The vial with cement paste was put into a sealed chamber under vacuum for 5 min to evacuate the air bubbles. For the acoustic measurement, after filling with paste, the sample mold was tapped on the bench 20 times to ensure the removal of air bubbles.

2.2. Chemical shrinkage test

The overall volume of hydrated (reacted) cement paste is smaller than the initial volume of solids and water, because the liquid water molecules become arranged into a more compact configuration in the hydrated phases. This reduction in volume is known as chemical shrinkage [25–27], and is reported as the measured volume reduction per gram of cement in the paste specimen during the hydration reaction (ASTM C1608). Chemical shrinkage is a measure of the rate and extent of hydration of cement pastes at early ages, comparable to the cumulative heat release measured by isothermal calorimetry [25]. A standard test method, ASTM C1608, is available for measuring chemical shrinkage.

There are two primary methods to measure chemical shrinkage. Geiker [25,26] devised a method of measuring the absorbed volume change of a liquid in contact with the paste specimen, as in ASTM C1608. Another method is to measure the change in density (or, buoyancy) of an immersed paste specimen in contact with water [27,28]. This paper utilizes a volume measurement in which the water level drop in a capillary tube due to chemical shrinkage is continuously determined by a sensitive differential pressure sensor (PX138 series from Omega with

a ±0.3 psi range and 0.5% typical and 1% maximum hysteresis). The accuracy of this measurement is ~1 mm water level change in the capillary tube. Around 12 g sample of cement paste was used in a glass vial with 25 mm diameter. The height of the sample is about 10 mm. For higher temperature tests, a smaller sample (8–10 g) was used to ensure that the change in volume was within the range of the capillary tube. The sample size used in this study is similar to that used in ASTM C1608. The experiment is performed under isothermal conditions by immersing the sample vial in a chamber provided with water circulation. An illustration of the experimental set-up is shown in Fig. 1. The design of this set-up is described in detail in [29]. The accuracy, repeatability, stability and applicability of this device have been confirmed [29]. However, there are some limitations of this apparatus. Due to the length limitation of the capillary tube used in this study, a maximum of 0.35 mL of water absorbed can be measured. When 12 g paste is tested, if w/c = 0.35, the maximum chemical shrinkage that can be measured is 0.04 mL/g, which is larger than the observed value within three days. Strong electromagnetic interference from the surroundings should be avoided, because it affects the pressure sensor reading; therefore, the sample chamber had to be kept ~1 m from the recirculating bath used for temperature control. The viscoelastic relaxation of the rubber stopper will affect the accuracy of the initial hour of data collection. Thus, the data reading starts one hour after mixing time. Also, the rubber stopper should be replaced frequently because of the aging problem of the rubber, especially at high temperature. Condensation in the pressure sensor at higher temperature could influence the sensor accuracy. At temperatures >40 °C, the data at late times (after 24 h for 60 °C) was noisy and unreliable. These errors could be avoided by improving the design of the apparatus.

2.3. Ultrasonic measurement

Ultrasonic wave velocities depend on the density and connectivity of the material being tested. An increase in material rigidity results in increased wave speed, so wave velocities change during cement hydration as the suspension evolves into an elastic solid. During the suspension period, the liquid phase is the dominant factor that determines the ultrasonic wave velocity. As cement grains gradually dissolve and hydration products nucleate, the connection of smaller particles leads to clusters that form a percolating solid network. The ultrasonic velocity shows a significant increase after the appearance of this network at the percolation threshold. The increase in compressive wave velocity measured at this time can be used to indicate the onset of structure formation and elastic property development (dynamic modulus) in cement systems. [30–32].

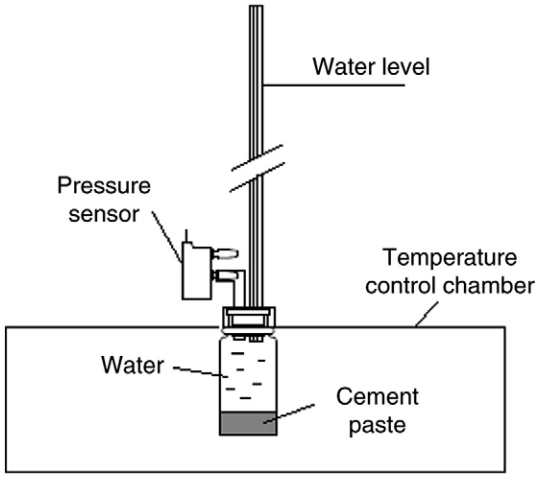

Fig. 1. Schematic of chemical shrinkage measurement system use in this study.

The experimental set-up used in this study consists of a two-channel acoustic emission system on a Peripheral Component Interconnect (PCI) card with 1 kHz–3 MHz bandwidth frequency response (Physical Acoustics Corporation). The design of the mold (Fig. 2) follows ref. [32]. Two piezoelectric transducers, a transmitter and a receiver, are mounted in plexi-glass plates facing each other, with a U-shaped copper plate placed in between, defining the volume to be occupied by the cement paste. The copper plate is surrounded by a cooling tube controlling the temperature. The device is secured by the use of screws, so the specimen can be easily demolded. The ultrasonic sensors are inserted in the walls, such that they are separated from the paste only by a 0.5 mm thickness of plexi-glass, so the reflection of the mold wall is minimized. The path length through the specimen (the distance that the wave travels through the paste) is 25 mm. To minimize the influence on the waves travelling through the mold but not the specimen, the diameter of the U-shaped plate is 70 mm. In general, a proper ultrasonic testing system has to fit the requirement that the wavelength must be small compared with the cross-sectional dimensions of the object being tested [33]. In this study, a frequency of 500 kHz was used, and the velocity in the cement sample normally varies from 500 m/s to 5000 m/s. The calculated wave length is 1–10 mm, so the dimensions of the apparatus meet the above requirement. The signal arrival time for velocities varying from 500 m/s to 5000 m/s is 5–50 μs, which is much larger than the time resolution, 0.1 μs. The accuracy of the measurement (error<1%) was confirmed by testing the wave velocity in standard materials, such as deionized water, aluminum, and brass. A layer of mineral oil was used to cover the top of the specimen to prevent water evaporation during the hydration and to minimize the loss of contact with the transducers due to the sample's decreasing volume. After casting the sample into the mold, the measurement is controlled automatically and the hydration time and the ultrasonic waves are recorded continuously at 1 min intervals.

2.4. Vicat setting time test

The Vicat setting test (ASTM C191) is the most commonly used method to identify the initial and final setting times for hydrating cementitious mixtures. It measures the change in the penetration depth of a plunger with a diameter of 1.13 ± 0.05 mm under a constant applied load (300 g) as increasing structure formation acts to reduce the extent of penetration into the specimen. The test identifies initial and final sets at penetration depths of 25 mm and 0.5 mm, respectively, for pastes having a normal consistency. At these penetration depths, the material has a shear resistance of about 32 and 900 kPa, respectively [34]. In this study, the paste was placed in wide-mouth polypropylene jars, with the same diameter as the standard mold that could be submerged in a water bath to control the hydration temperature. A specific concern regarding the Vicat test is that the times of initial and final set assessed using this technique are somewhat arbitrarily defined and may not correspond to a specific aspect of structure formation in the system. In this study, only the initial setting time was assessed for cement pastes using this technique.

2.5. Thermogravimetric analysis

Thermogavimetric analysis (TGA) is a technique that measures the progressive weight loss of a sample as it is being heated at a controlled rate. A change in mass within a specific temperature range identifies the presence of particular chemical compounds. The magnitude of the change in mass indicates the amount of the compound in the sample. For cement paste, the amount of product that is burned allows one to measure the degree of hydration, α [35,36]:

$$\alpha = \frac{W_n}{0.23} - LOI \quad (1)$$

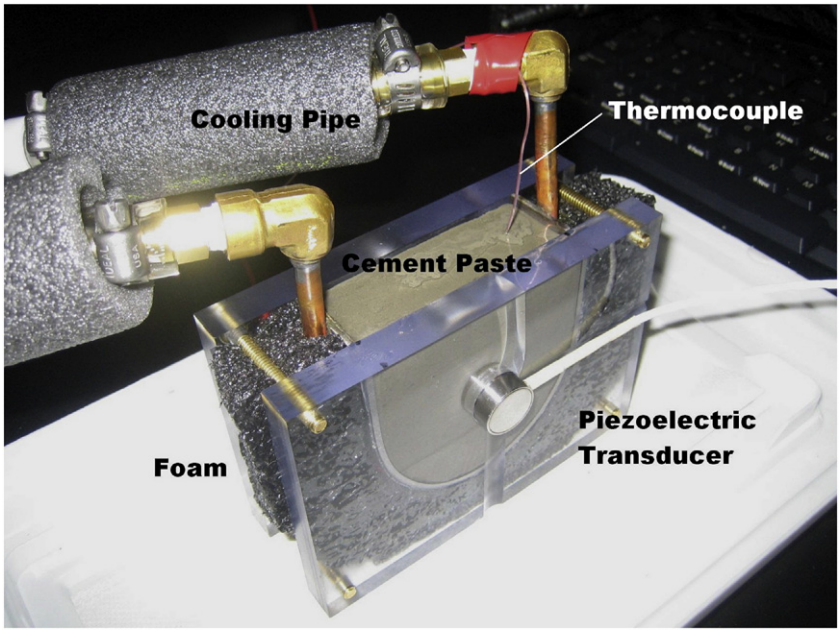

Fig. 2. Picture of mold with cement paste sample inside in ultrasonic measurement system.

where

$$W_n = \frac{W_{105^\circ C} - W_{1000^\circ C}}{W_{1000^\circ C}} \quad (2)$$

Here, W_n is the normalized weight loss of the hydrated sample and LOI (Loss On Ignition) is the normalized weight loss of the unhydrated cement. The factor of 0.23 in Eq. (1) represents the non-evaporable water content per gram of cement in the mixture for complete hydration. It is an estimated value calculated based on the Bogue composition of cement and the Molina coefficients [35]. For most Portland cements, this value is generally somewhere between 0.23 and 0.25. The degree of hydration, α, may relate either to an individual clinker phase or to the cement as a whole, and it can be problematic to determine, because cement is a mixture of phases that react at different rates. Therefore, it is generally accepted that the so-called degree of hydration of cement is an overall and approximate measure [37]. It is defined here as the mass fraction of the cement that has reacted, irrespective of phase.

To determine the degree of hydration as a function of time, it was necessary to arrest the chemical reaction of samples removed from the paste. This can be done by solvent exchange, but this can result in chemical reactions between the paste and the solvent (see review in ref. [38]). In this study, hydration was quenched by immersing small samples (~5 g for each sample) of hydrating paste into liquid nitrogen (−195 °C) for more than 15 min. After freezing, the samples were immediately placed in a freeze-dryer in which the temperature and vacuum were kept at −77.7 °C and 4 Pa, respectively [38]. Three days were usually needed to dry the samples. Then, the freeze-dried samples weighing about 50 mg were heated to 105 °C and held for a half hour, then heated to 1000 °C at a rate of 10 °C/min. The normalized weight loss between 105 °C and 1000 °C was used to calculate the degree of hydration.

3. Results

3.1. Chemical shrinkage

The chemical shrinkage of cement pastes with w/c = 0.35 and cured at various temperatures (10, 25, 40 and 60 °C) is plotted versus the hydration age (i.e., time since initial contact with water) in Fig. 3. The shrinkage of the system is continuously recorded for three days, starting 30 min after water–cement contact, because 30 min is necessary for mixing, casting and temperature stabilization. Increase in temperature causes an increase in the rate of chemical shrinkage, as was found by Mounanga et al. [28]. At higher temperatures, the sample reaches the plateau in shrinkage faster. At later ages, the curves corresponding to different temperatures cross. Fig. 4 shows the chemical shrinkage data at different w/c for a given temperature. The curves are identical at the beginning, but separate after the appearance of the plateau and will never cross. Fig. 5 illustrates the influence of additives on the chemical shrinkage. At the same curing temperature and w/c, various types and dosages of additives change the hydration rate. Increased concentration of an accelerator, $CaCl_2$, (from 0.3 to 1.5% of the mass of cement) accelerates the hydration and the evolution of chemical shrinkage. Pastes with retarder, fluid-loss control agent and viscosity modifying agent show slower hydration. After approximately 20 h, the shrinkage in the samples with HEC and DT is accelerated, which indicates that while the fluid-loss control agent or viscosity modifying agent retard hydration, they have an accelerating effect at the later ages.

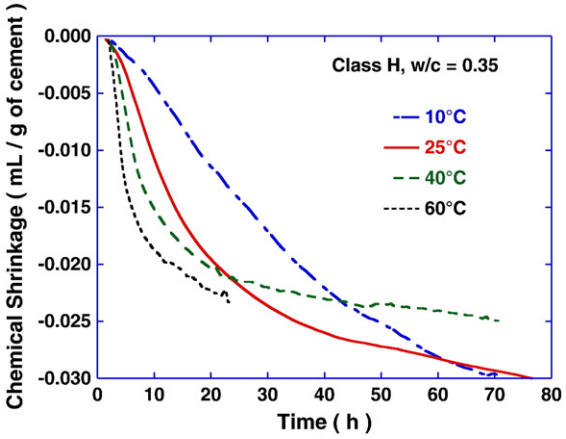

Fig. 3. Chemical shrinkage versus time for Class H cement pastes with w/c = 0.35 and cured at 10, 25, 40 and 60 °C. The sample at 60 °C was only measured for one day because the condensation in the sensor caused by the high temperature made the result noisy and unreliable.

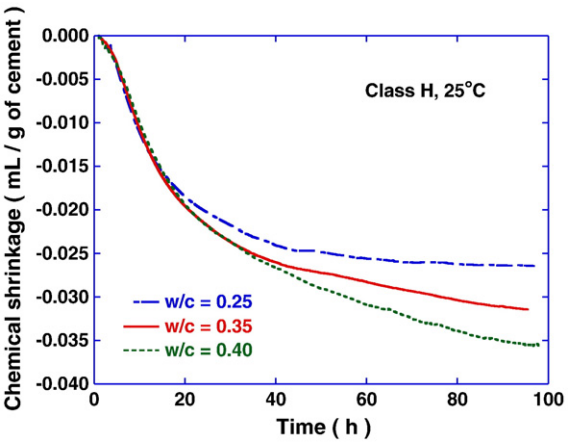

Fig. 4. Chemical shrinkage versus time for Class H cement pastes with w/c = 0.25, 0.35 and 0.40, and cured at 25 °C.

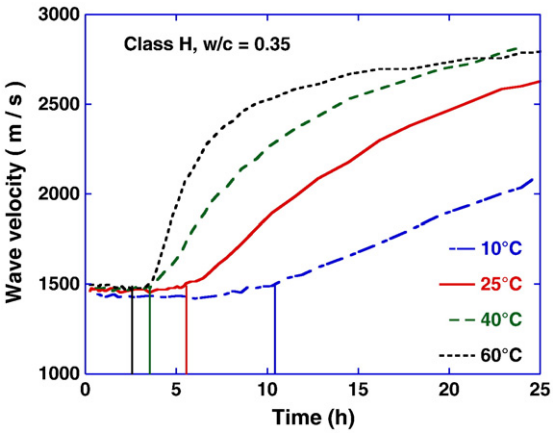

Fig. 6. Ultrasonic wave velocity versus time for Class H cement pastes with w/c = 0.35 and cured at 10, 25, 40 and 60 °C. The vertical straight lines indicate the initial setting time determined by Vicat test (10.75, 5.5, 3.33 and 2.25 h for samples cured at 10, 25, 40 and 60 °C, respectively).

3.2. Setting time

The ultrasonic wave velocity versus hydration age for Class H cement pastes is shown in Figs. 6–8, in which initial setting times determined by Vicat test are also indicated. Traditionally, cement setting time is determined by the Vicat test, which measures the decrease of the needle penetration into the specimen with increasing structure formation. Alternatively, ultrasonic testing, in which a high-frequency wave is propagated through a sample, can be used to assess the setting time. The velocity of the ultrasonic wave increases as the cement hydrates. All the curves in Figs. 6–8 behave similarly. Initially, the velocity is constant and equal to the wave velocity in water (~1500 m/s), because the cement paste is a suspension of cement particles in water, and the preferential propagation medium is the liquid. In the cement paste with w/c = 0.25 in Fig. 7, the initial velocity is lower than 1500 m/s, because the paste in the acoustic measurement was not de-aired and a number of tiny air bubbles were trapped in the paste, so the preferential propagation medium contains air in which the velocity is 340 m/s. Fig. 6 shows the obvious increase in the rate of ultrasonic velocity development with increasing temperature. Fig. 7 shows the ultrasonic velocity results for the cement pastes with different w/c. Except for w/c = 0.25, where the compressional wave velocity at early ages is influenced by the presence of air in the system, all the other samples have similar initial values (about 1500 m/s). After the set point, the samples with lower w/c exhibit faster velocity increase and higher final values. In Fig. 8, the effect of retarder on cement setting and hydration is the most clear. The curve for the sample with 0.05% MD and 0.25% DT2 highlights the advantage of the automated ultrasonic method when delayed setting occurs.

3.3. Degree of hydration

Fig. 9 displays the degree of hydration of Class H cement pastes isothermally hydrated at temperatures between 10 °C and 60 °C. More product is formed at any given time as the temperature increases, which correlates with the chemical shrinkage (Fig. 3) and ultrasonic wave velocity (Fig. 6) behaviors. On the logarithmic scale of hydration time, it is obvious that the initial hydration rate is very slow, corresponding to hydration Stage II (induction period) [39]. After the setting time, α begins to increase rapidly. The horizontal line labeled "Initial set" in Fig. 9 indicates a nearly constant value of degree of hydration at the initial setting time (Vicat) for the mixtures evaluated in this study. Results for samples with additives further demonstrate that there is a characteristic value for α at the setting time for samples of Class H cement isothermally hydrated between 10 °C and 60 °C, with and

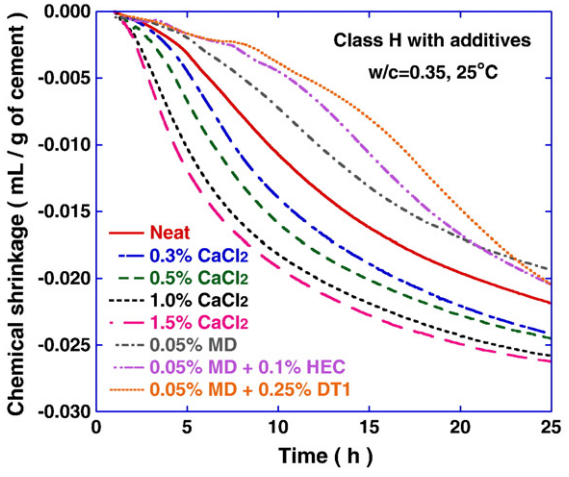

Fig. 5. Chemical shrinkage versus time for Class H cement pastes with indicated additives, w/c = 0.35, and cured at 25 °C. The additives include accelerator calcium chloride ($CaCl_2$), retarder maltodextrin (MD), and dispersants hydroxyethylcellulose (HEC) and diutan (DT). Indicated wt.% is relative to the mass of cement.

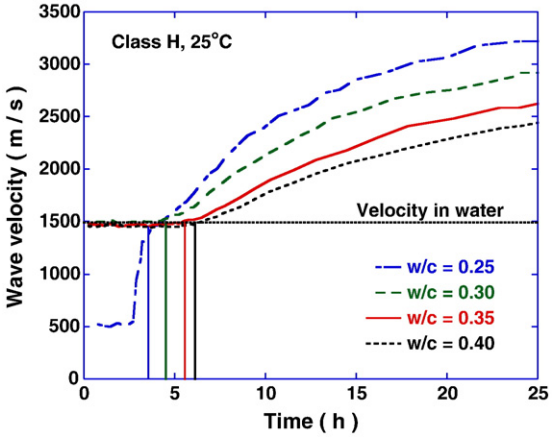

Fig. 7. Ultrasonic wave velocity versus time for Class H cement pastes with w/c = 0.25, 0.30, 0.35 and 0.40, and cured at 25 °C. The vertical straight lines indicate the initial setting time determined by Vicat test (3.75, 4.67, 5.5 and 6 h for samples with w/c = 0.25, 0.30, 0.35 and 0.40, respectively). The wave velocity in water is 1497 m/s at 25 °C. Sample with w/c = 0.25 has lower initial velocity because of air bubbles were trapped in the sample which should be avoided by using vacuum mixing.

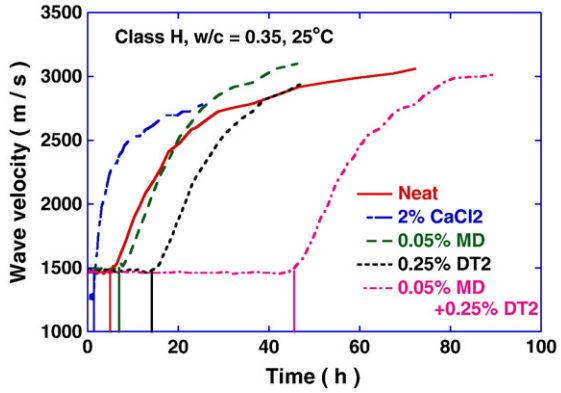

Fig. 8. Ultrasonic wave velocity versus time for Class H cement pastes with different additives, w/c = 0.35, and cured at 25 °C. The solid straight lines indicate the initial setting time determined by Vicat test. Sample with 2% $CaCl_2$ has lower initial velocity because of air bubbles were trapped in the sample which should be avoided by using vacuum mixing.

without additives, at a given w/c = 0.35. This value is approximately $\alpha = 3.88 \pm 0.38\%$, although the setting time changes from 2.25 h to 15.55 h for different samples. If dispersants, such as superplasticizers, are added in the mixture, the cement particle spacing increases and a higher value of α might be needed to cause percolation and setting. As long as the cement paste has a similar particle size distribution and spacing, the thickness of the hydrates on the particles at the setting point should be the same.

4. Discussion

4.1. Chemical shrinkage and degree of hydration

In the plots of chemical shrinkage versus hydration age shown in Figs. 3–5, the behavior of the curves is similar. The slope of the chemical shrinkage is very slow during Stage II in the cement hydration. This period is shorter in accelerated pastes, such as those at higher temperature or with $CaCl_2$ additions. Because the chemical shrinkage measurement could not start recording the data until half an hour after mixing (allowing time for mixing, casting and temperature stabilization), Stage I was not observed. The C_3A content in Class H cement is quite low, so the fast C_3A reaction at the beginning of hydration can be neglected. However, for ordinary Portland cement, Beltzung and Wittmann [40], and Sant et al. [27] noticed a rapid initial increase in chemical shrinkage caused by the reaction of C_3A. During the induction period, the rate of chemical shrinkage is low, but measurable. As the cement paste approaches the setting point determined by other methods that will be described in detail later in this paper, the hydration enters Stage III (acceleration period), and the chemical shrinkage begins to increase rapidly. There is no obvious critical point in the chemical shrinkage curve at which the hydration transforms from Stage II to Stage III. The slope rises gradually and the change is not as obvious as in calorimetry curves. Other chemical shrinkage results [41–44] also showed a similar trend. The cause of the induction period and of its termination has been the subject of much debate. One suggestion is that the product of the initial reaction forms a protective thin hydrated layer on the C_3S particles that acts as a diffusion barrier to dissolving ions; this is broken or rendered more permeable by aging or phase transformation [3,45,46]. Another thought is that there is no barrier layer and the kinetics is explained by the difficulty in nucleating calcium silicate hydrate gel (C–S–H) [47,48]. In any case, the rate of reaction in the induction and acceleratory periods is controlled by nucleation and growth of the C–S–H: the induction period ends when the volume fraction of product increases rapidly. Both the maximum rate of reaction and the time at which it occurs depend strongly on the temperature and additives, while they are independent of the w/c. It can be seen that the higher temperature specimens and the samples with accelerators have steeper slopes in the chemical shrinkage curve. The curves of pastes with different w/c are close before 12 h of hydration, at which time the curves start a plateau. In some rapidly hydrated specimens, the chemical shrinkage curve shows a plateau with a small slope corresponding to the decelerated hydration in Stage IV. The early hydration period is generally considered to comprise stages I–IV.

There is a linear relationship between chemical shrinkage (ΔV) and the degree of hydration (α), as shown in Fig. 10. Companion samples from the same batch of cement paste that was used in the chemical shrinkage measurement were quenched at time intervals, and α was calculated from the TGA results using Eq. (1). Thus, each α at a certain hydration time has a corresponding chemical shrinkage value. Curves of α versus t will be described as kinetic curves. In principle, degree of hydration may be obtained by summing the amounts of the individual phases that have reacted. Owing to the experimental difficulty and questionable precision of such approaches (e.g., quantitative X-ray diffraction), less direct methods have often been used, based on the determination of such quantities as non-evaporable water, or cumulative heat evolution. Our results show that chemical shrinkage is proportional to the degree of hydration. Given this relationship, chemical shrinkage is regarded as "an index to the progress of the reactions" [49].

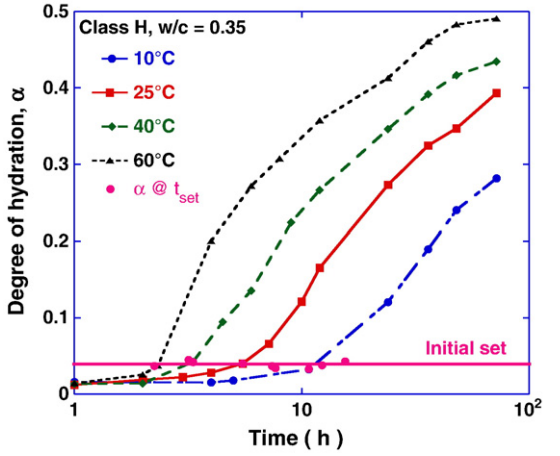

Fig. 9. Degree of hydration, α, calculated from Eq. (1), versus log of hydration age for freeze-dried samples from Class H cement pastes with w/c = 0.35. The curves are from samples isothermally hydrated at 10, 25, 40 and 60 °C; hydration was quenched at times up to 72 h. Dots on the line labeled "Initial set" show α at the initial setting time for samples with 0.05% MD, 0.25% DT1, 0.05% MD + 0.1% HEC, 0.05% MD + 0.25% DT1, and 0.5% $CaCl_2$. The initial setting time varies from 2.25 to 15.55 h for different specimens.

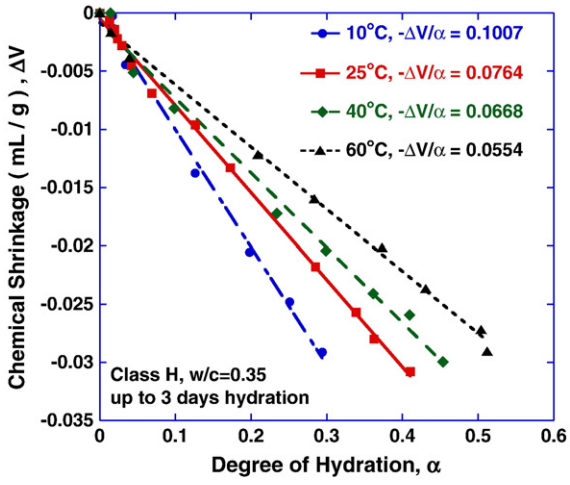

Fig. 10. Linear relationship between chemical shrinkage and degree of hydration during the first 72 h of hydration for cement pastes (Class H, 25 °C, w/c = 0.35) at $T = 10, 25, 40$ and 60 °C.

Fig. 3 shows that increase in temperature causes an increase in the rate of chemical shrinkage. Therefore, at higher temperatures the precipitation starts earlier and the chemical shrinkage reaches a plateau faster. Rapid hydration at high temperature leads to encapsulation of the cement grains by a dense product layer of low porosity [50,51], which retards further hydration. The effects of curing temperature on hydration kinetics have been shown to be two-fold. On the one hand, the reaction rate increases with the increase in temperature [52,53]. On the other hand, the packing of the hydrates becomes denser at higher temperatures [19,54,55], which slows down the further hydration. Therefore, during the late period, the hydration rate is lower at elevated temperature and the ultimate degree of hydration may thus also be lower [56]. From Fig. 3, the curves corresponding to different temperatures cross at later ages. From the trends, for the w/c examined here, the ultimate chemical shrinkage decreases with the increase of temperature which is consistent with the findings of Geiker and Knudsen [26].

The initial hydration rate is independent of the w/c as shown in the chemical shrinkage curves in Fig. 4, because the particles are initially surrounded by water, even at the lowest w/c used here. Therefore, the degree of hydration, as well as the chemical shrinkage, is only controlled by the nucleation and growth of hydration products, independent of the distance between particles at different w/c. With increasing reaction, the hydration products eventually cause disconnection of the pores, resulting in a pore network depercolation threshold. This may be responsible for the obvious divergence in the chemical shrinkage rate, as depercolation of the pore structure makes it more difficult for the water to reach the cement [25]. Samples with lower w/c reach a plateau faster, but have a smaller chemical shrinkage at later ages due to the overlapping layers of hydration product constituting a barrier to reaction. Beyond this point, the reaction rate may be controlled by diffusion, rather than nucleation and growth, but the time of that transition is not revealed by our data.

Fig. 10 shows that chemical shrinkage and degree of hydration have a linear relationship with a slope that becomes less negative as temperature increases. Thus, at the same degree of hydration, higher temperature causes smaller chemical shrinkage [25,28]. This may be caused by the decreasing density of the cement hydrates at higher temperature [55,57]. Thomas et al. [57] found that the C–S–H has a lower skeletal density at higher temperatures, although the porosity of the C–S–H decreases. Extrapolating the linear fits in Fig. 10, the ultimate chemical shrinkage of Class H cement at $\alpha = 1$ is found to decrease with increasing temperature, from 0.101 mL/g at 10 °C to 0.0554 mL/g at 60 °C. This trend is in good agreement with the results of Geiker and Knudsen [26], who reported that the chemical shrinkage of OPC paste (w/c = 0.5) decreased from 0.0530 mL/g to 0.0338 mL/g with increasing temperature from 20 °C to 50 °C. The ultimate chemical shrinkage values calculated from the curving fitting in Fig. 10 are slightly overestimated for the Class H cement, because at early ages more of the C_3S reacts, and then at later hydration stages more C_2S reacts. Based on the measured density of the C–S–H hydration products, Thomas et al. [57] calculated the chemical shrinkage values to be about 0.0618 mL/g for complete hydration of C_3S and 0.0489 mL/g for complete hydration of C_2S, respectively. In this study, the fitted data are from the first three days of hydration, where C_3S dominates the reaction. Although the extrapolations for the total chemical shrinkage from Fig. 10 are known to be high, they are in the same range as in the previous results [26,57]. Geiker [25] and Sant et al. [27] observed that increasing total sample size caused a reduction in chemical shrinkage at later ages and that this was amplified in specimens with a lower w/c or finer cement, because these factors favor self-desiccation. In the present study, the thickness of paste is small enough (~10 mm thick), so self-desiccation is not likely to happen [58]. Moreover, the formation of denser shells at higher temperature would lead to less, not more, self-desiccation, because it leaves the capillary porosity more open. In other words, the permeability of the specimen would be higher at higher temperatures, making it easier for the water to get into the specimen and avoid self-desiccation.

4.2. Degree of hydration at the setting point

Hydration products spread over the surfaces of the cement particles and eventually begin to bind the particles together. The solid network continues to develop until it becomes connected throughout the material. At this critical time, a solid percolation path is formed. Therefore, the ultrasonic wave path switches from the liquid phase to the solid phase, which leads to a significant increase in wave velocity, as shown in Figs. 6–8. This critical point, when the system changes from a suspension of cement particles in water to an interconnected solid phase, can be regarded as the solid percolation threshold (setting point) [59]. The increase in the ultrasonic velocity corresponds to the onset of elastic properties in the solid materials, such as bulk and shear moduli [6]. After a solid structure has developed, the transmission velocities in the pastes show a similar trend. This increase in velocity roughly coincides with the initial setting time as assessed by the Vicat test. It has been reported [34] that the percolation threshold occurs prior to the initial setting time defined by the Vicat test, which happens when the material already has a yield stress of about 32 kPa. Therefore, the critical point of increase in velocity corresponds more closely to the end of the induction period in cement hydration for most of the mixtures, when the rate of cement hydration begins to increase [30,60]. In our study, only a small offset (less than 10 min) has been noticed between the initial setting time from the Vicat test and the percolation threshold found from the acoustic measurement.

Fig. 6 presents the effect of temperature on the ultrasonic velocity during hydration. As expected, the sample with higher temperature has a quicker increase in the velocity and reaches a plateau faster. In other words, the increase of temperature causes faster setting and an accelerated development of hydration. Similarly to the chemical shrinkage curves (Fig. 3), wave velocity curves at higher temperature reach the plateau faster and the curves for different temperatures cross at later ages. At 24 h, the velocity in the 40 °C sample exceeds that in the 60 °C sample. Wave velocity in more porous materials is lower. This is an important point as it confirms that an increase in curing temperature serves to reduce the density of the cement hydrates and increase the porosity of the system [55,61]. In pastes hydrated at higher temperature, it is reported that the hydration products are less uniformly distributed than in those hydrated at lower temperature [50,51], and larger pores are present in the interstitial space [3,51,62]. Thus, hydration rates increase remarkably with temperature, but the ultimate strength is generally reduced [62]. By decreasing w/c, the sample exhibits faster velocity increase and higher final values, as shown in Fig. 7. This presumably reflects the increased number of particle contacts at lower w/c, which enables the hydration products to bind the particles more efficiently at a lower degree of hydration. The combination of the retarder MD and the viscosity modifying agent DT significantly retarded the setting time (in Fig. 8). The lower initial velocity of the sample with $CaCl_2$ occurs because the $CaCl_2$ is an accelerator that increased the plastic viscosity of the paste. Consequently, during the mixing and casting, air bubbles may be trapped in the paste to influence the initial velocity. To avoid this, vacuum mixing is recommended.

It is important to identify the amount of reaction products (degree of hydration) needed to develop a percolated solid structure in cementitious materials. The physical development of a solid network depends on the particle spacing (w/c, dispersant) and the particle size (fineness, and size distribution). For a given w/c and cement fineness, the percolation threshold (setting point) of the slurry corresponds to a specific degree of hydration of the cement, regardless of the temperature, pressure and accelerating/retarding agents. Fig. 9 confirms this by showing the identical degree of reaction at the setting time for specimens with the same w/c, but hydrated at various temperatures and with different retarders and accelerators. This also proves the basic assumption in the model to predict the influence of temperature and pressure on the rate of hydration discussed in [4].

Fig. 11 schematically illustrates the particle spacing effect in two systems having different w/c. The amount of hydration products needed

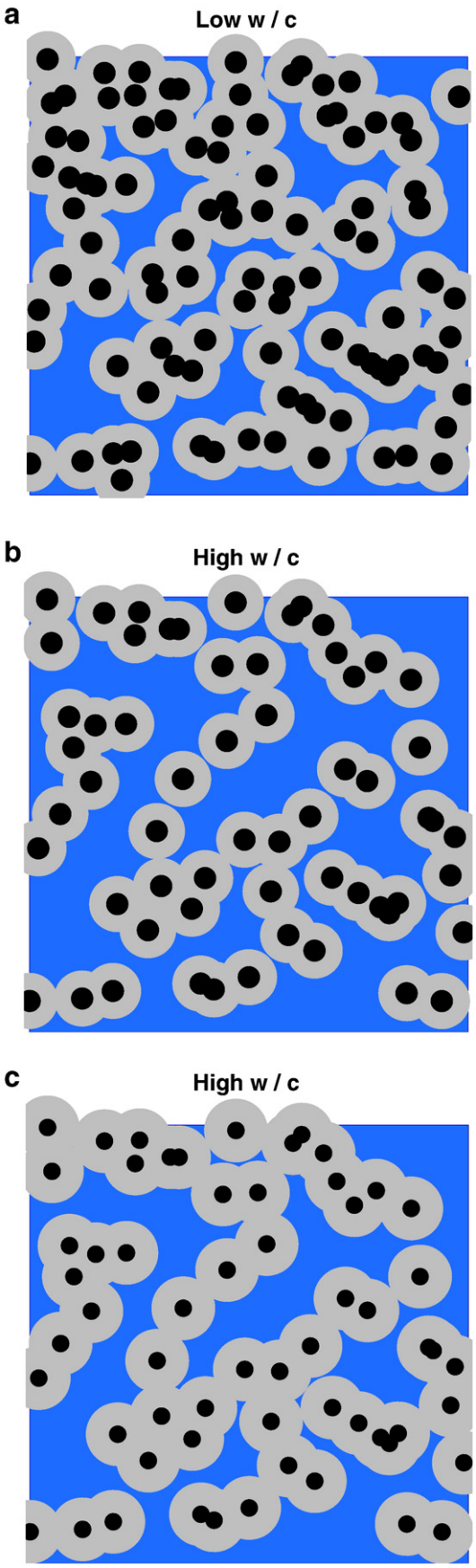

Fig. 11. Schematic illustration of solid phase percolation at setting for different w/c. Matrix is filled with water (blue), black particles are cement grains, and gray shells represents the hydration products. (a) Contiguous gray shells indicate that the hydration products have percolated, so this material (with relatively low w/c) has set; (b) at the same degree of hydration as in (a), this higher w/c has not set; (c) at a higher degree of hydration, the sample with the same w/c as in (b) has set.

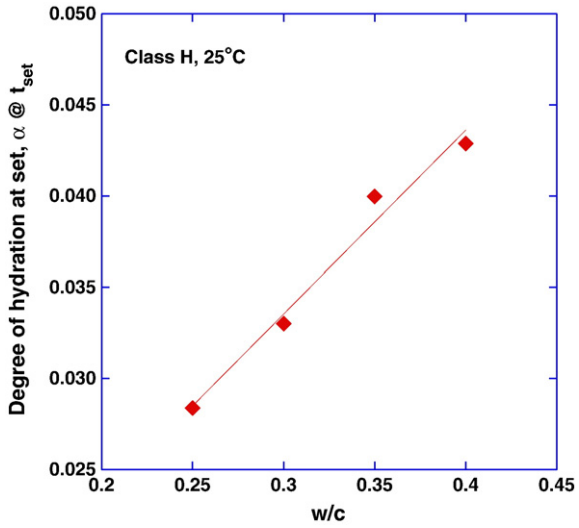

Fig. 12. Degree of hydration at setting time versus water/cement ratio.

to develop a percolating structure is greater in the higher w/c system, which has larger solid-to-solid spacing. Consequently, the system with lower w/c needs a smaller volume of hydration products to form a stress-resisting network. To verify this, the degree of hydration at the setting time was measured for specimens with w/c varying from 0.25 to 0.40. Fig. 12 shows a linear relationship between w/c (related to particle spacing) and degree of hydration at setting (amount of hydration products required for solid percolation). Higher w/c requires more products to cause percolation.

4.3. Boundary Nucleation and Growth (BNG) model and setting time prediction

It is possible to interpret hydration kinetics using Avrami-type equations [14–16], which describe an isothermal phase transformation that occurs within a fixed volume by a nucleation and growth process. The standard Avrami model gives the transformed volume fraction, X, at time, t, in terms of two parameters, k (effective rate constant) and n (exponent):

$$X = 1 - \exp\left[-(kt)^n\right] \tag{3}$$

Avrami's theory assumes that nucleation occurs at randomly distributed locations within the untransformed volume. Cahn [17,18] modified this to allow the nuclei to form on the surfaces of particles (grain boundaries) and then grow into the grains. In the case of hydration, the "grains" are the water-filled interstitial spaces where the hydration products form. Consider an untransformed volume containing a single planar boundary, and assume that nucleation of the transformed phase occurs only at spatially random locations on this boundary. A spherical region that nucleated at time τ and grows at rate G will intersect with this plane at time t in a circle with area $\pi[G^2(t-\tau)^2 - y^2]$ if $t > \tau + y/G$. (If $t < \tau + y/G$, the region of transformed phase has not yet reached the plane and the area is zero.) The hydration product nucleates on the particles with surface area O_v^B (area per unit paste volume) at the rate I_B (nuclei per unit area of

boundary per time); if the growth rate, G (m/s), is assumed to be constant and isotropic, the result is

$$X = 1 - \exp\left[-2O_v^B \int_0^{Gt} (1 - \exp(-Y^e))dy\right] \quad (4)$$

where

$$Y^e = \begin{cases} \frac{\pi}{3} I_B G^2 t^3 \left(1 - \frac{3y^2}{G^2t^2} + \frac{2y^3}{G^3t^3}\right) & (\text{if } t > y/G) \\ 0 & (\text{if } t < y/G) \end{cases} \quad (5)$$

Thomas [8,57] applied this mathematical model to calorimetric data to describe the C_3S hydration process and rewrote the Boundary Nucleation and Growth (BNG) model in terms of two independent rate constants: k_B describes the rate at which the nucleated boundary area transforms (particle surfaces become covered with hydration product), and k_G describes the rate at which the "grains" between the boundaries grow (that is, capillary pore space between the particles fills in with product). They have units of inverse time and are given by

$$k_B = \frac{\left(I_B O_v^B\right)^{1/4}}{G^{3/4}} \quad (6)$$

and

$$k_G = O_v^B G \quad (7)$$

If any of the three parameters in Eq. (4), O_v^B, I_B, and G, can be determined independently, then the other two can be calculated from the fitted values of the rate constants in Eqs. (6) and (7). Given the surface area of the cement measured by the BET method (1 m^2/g), we can calculate O_v^B.

When applying the BNG model to hydration data (calorimetry or chemical shrinkage), where the degree of transformation is F, one additional parameter is needed: the total change (heat or shrinkage) per unit volume of material transformed, A. The above Eqs. (6) and (7) can be written as:

$$F(t) = A\{1 - \exp[-2k_G t(1 - f_Y(t))]\} \quad (8)$$

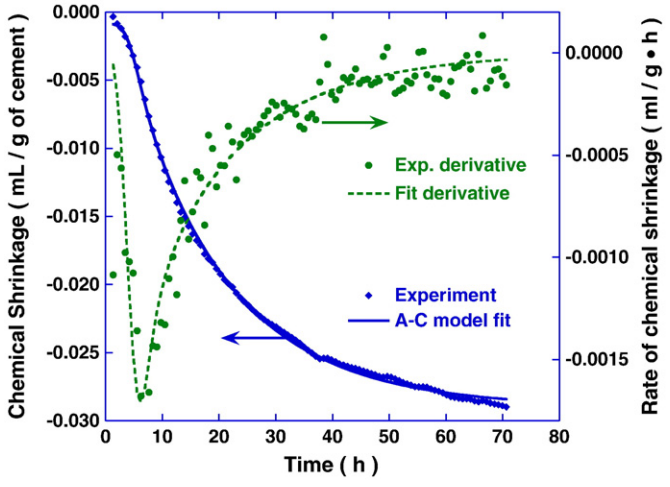

Fig. 13. Chemical shrinkage experimental data and the fitting by BNG model (left axis); rate of shrinkage and fit (from numerical derivative of data and analytical derivative of fit, respectively).

where

$$f_Y(t) = \begin{cases} \frac{\pi}{3}\frac{k_B^4}{k_G} \int_0^1 \exp\left[-t^3\left(1 - 3x^2 + 2x^3\right)\right]dx & (\text{if } x<1) \\ 1 & (\text{if } x > 1) \end{cases} \quad (9)$$

where $x = y/(Gt)$. Thomas [8,57] used one more parameter in his fitting; the effective starting time, t_0. If the nucleation rate is faster at the start of the reaction (in contradiction to the constant I_B assumed in the model) or if some nuclei form rapidly at the time of mixing, then the fit may yield a negative value of t_0. If the nucleation rate is slower at the start of the reaction, or if nucleation is inhibited initially in the induction period, then t_0 will be positive. Whether t_0 is positive or negative is determined by fitting the experimental data; results in the literature [8,63] indicate no obvious relationship between t_0 and the cement's physical properties. In this study, we assume that the nucleation and growth start when water contacts the cement (i.e., the reaction begins at mixing time) and the nucleation begins at a constant rate at that time, so $t_0 = 0$.

We now apply this model to the chemical shrinkage during Class H cement hydration. Class H cement contains C_3S, C_2S, C_3A and C_4AF as its four major clinker phases (as shown in Table 1). In contrast to ordinary Portland cement, Class H cement has a negligible amount of C_3A which is well known to have the fastest reaction and to control the very early hydration. It can be reasonably assumed that the reaction of C_3S dominates the early hydration. Therefore, the boundary nucleation equation can be applied to describe the hydration process, such that continuous nucleation occurs on the cement particle surfaces and the rate of growth of the hydration product is constant with time. For a cement with a considerable amount of C_3A, because the early hydration includes more complicated reactions, the BNG model might not apply, as the growth

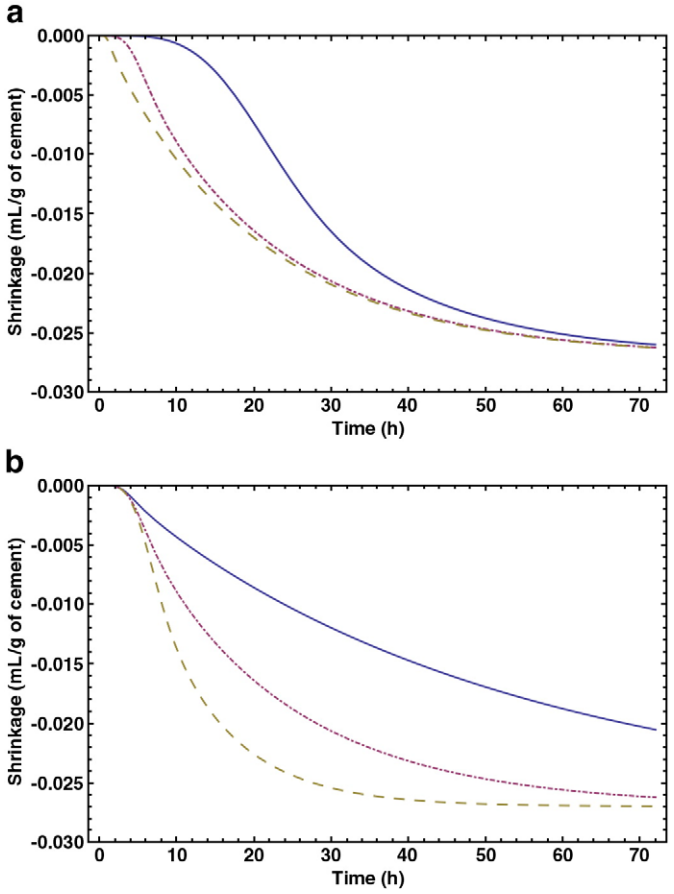

Fig. 14. Response of the BNG curve when k_B and k_G change.

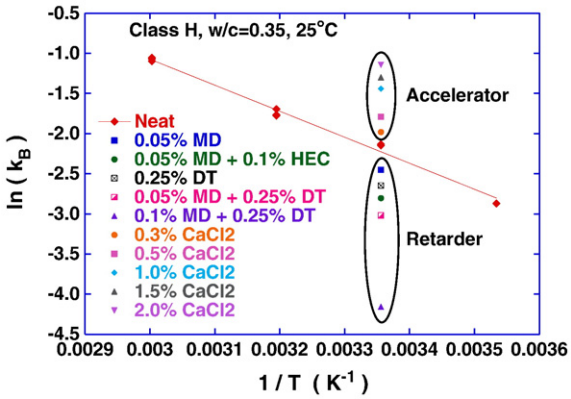

Fig. 15. Nucleation parameter k_B versus reciprocal temperature.

rate might not be constant. Fig. 13 shows a typical BNG fit, indicating that the model successfully describes the chemical shrinkage data for Class H cement until well beyond the peak in the hydration rate.

At long times, Eq. (8) approaches:

$$X(t) = \frac{F(t)}{A} \approx 1 - \exp(-2k_G t) \tag{10}$$

If we can measure the whole hydration process, a fit to this expression can be used to determine the parameters A and k_G. However, in this study, we focused on the early hydration and only measured the chemical shrinkage up to 72 h. Based on the TGA result in Fig. 9, the degree of hydration only reaches 50% at 72 h for the fastest hydration conditions (*viz.*, 60 °C). Therefore, to accurately estimate parameters A and k_G from our chemical shrinkage data is practically impossible.

Fig. 14 shows how changes in k_B and k_G affect the shape of the chemical shrinkage curve: k_B predominantly affects the initial hydration, while the growth rate, k_G, predominantly affects the later hydration. However, cement hydration eventually becomes diffusion-controlled, so the growth rate becomes dependent on time. At that point, the present form of the BNG model is no longer valid. For this reason, only k_B was analyzed in this paper.

Fig. 15 shows that k_B has an Arrhenius-type dependence on temperature with an activation energy of 32.5 kJ/mole. It increases with increasing temperature and addition of accelerator. Higher temperature and accelerators result in faster nucleation and growth rates, leading to earlier percolation of hydration products.

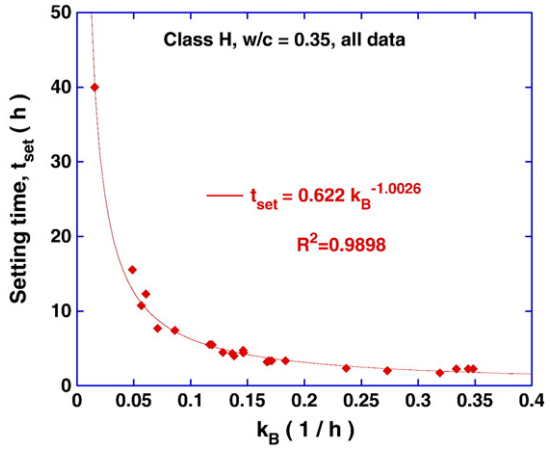

Fig. 16. Nucleation parameter k_B versus setting time of all the samples at various temperatures and with additives at a given w/c = 0.35. Setting time and k_B have an inverse relationship which confirms that the amount of hydration product at the setting point is a constant.

For a given specimen, k_B is a constant, so it can be used to calculate the amount of the product at a given time. For different specimens, k_B is influenced by the ambient temperature, pressure and additives. Our result shows that the amount of hydration products is the same for a given w/c at the setting time. When the degree of reaction is small, Eq. (8) reduces to:

$$X(t) = \frac{F(t)}{A} = 1 - \exp\left[-2k_G t\left(1 - \int_0^1 \exp\left[-\frac{\pi}{3}\frac{k_B^4}{k_G}t^3\left(1-3x^2+2x^3\right)\right]dx\right)\right]$$
$$\approx 2k_G t \int_0^1 \frac{\pi}{3}\frac{k_B^4}{k_G}t^3\left(1-3x^2+2x^3\right)dx \approx \frac{\pi}{3}k_B^4 t^4 \tag{11}$$

This is a reasonable approximation at the setting point. We can rearrange Eq. (11) to find the setting time when the amount of hydration at setting time, X_{set}, is known:

$$t_{set} \approx \left(\frac{3}{\pi}X_{set}\right)^{1/4} k_B^{-1} \tag{12}$$

Fig. 16 shows the relationship between k_B and the initial setting time found by the Vicat method. A higher nucleation rate corresponds to faster setting. The fit in Fig. 16, matches well with the prediction of the BNG model, Eq. (12): t_{set} and k_B have an inverse relationship with a proportionality constant that is expected to be related to the amount of hydration products. Therefore, the amount of hydration products at the setting time can be calculated. From the fitting equation in Fig. 16, X_{set} is 15% of the transformed volume fraction, which is larger than the TGA result, 3.88%. There are two reasons for this discrepancy in the proportionality factor in Eq. (12). First, there is a factor 2 inside the exponential function in Eq. (8), which corresponds to an equal growth rate in both directions on the nucleation surface. However, generally we expect the growth rates into the interstitial space to be faster than the penetration of the hydration products into the particles, so the factor of 2 should be replaced by a number between 1 and 2. This will be discussed in the forthcoming paper. The second problem is that the approximation in Eq. (11), which leads to Eq. (12), is not precise at the setting point. Nevertheless, the experimental results confirm the prediction of an inverse relationship between k_B and t_{set}. Given that the amount of hydration product is constant at the setting point, Eq. (12), provides satisfactory predictions of the setting time for mixtures cured at different temperatures and pressures [4]. The discrepancy between the observed and predicted values of X_{set} in Fig. 16 does not compromise the prediction of setting time significantly, because the reaction is accelerating rapidly at that point, so the difference in X corresponds to a short interval of time. Moreover, if a single value of X_{set} is known, it can be used to precisely predict the setting time at other temperatures or with other additives.

5. Conclusions

Temperature increase and calcium chloride additions accelerate the rate of cement hydration, causing earlier setting; conversely, retarder maltodextrin, and the additives hydroxyethylcellulose and diutan delay cement hydration, causing later setting times.

Setting is a percolation process. Consequently, for the mixtures evaluated, at a given w/c, the degree of hydration at setting is a constant, regardless of the effects of ambient temperature or presence of additives. A lower w/c paste needs a smaller amount of hydration product (lower degree of hydration) to form a percolating solid network.

Vicat needle penetration and ultrasonic wave velocity tests correspond well, as they are both sensitive to the development of a stress-resisting (percolating) network. Ultrasonic velocity measurements can replace the Vicat test for accurate and convenient determination of the setting time.

TGA analysis confirms that chemical shrinkage and degree of hydration are linearly related.

The initial hydration of cement follows the Boundary Nucleation and Growth (BNG) model, assuming constant rates of nucleation and growth. There is a reciprocal relationship between the parameter k_B and the setting time. Given that the amount of hydration product is constant at the setting point, when k_B is known, setting time can be predicted [4]. In a forthcoming publication, we will explore an alternative formulation of the BNG model in which growth occurs from a fixed number of nuclei. That model also shows excellent agreement with the data, and has certain theoretical advantages [8].

Acknowledgements

The authors gratefully acknowledge the financial support provided by Halliburton. The authors also thank Mr. Joseph Vocaturo for his assistance in designing and setting up the chemical shrinkage device.

References

[1] D.K. Smith, Cementing, Revised ed., Society of Petroleum Engineers Inc., Compliments of Halliburton Services, Richardson, TX, 1990.
[2] E.B. Nelson, D. Guillot (Eds.), Well Cementing, 2nd ed, Schlumberger, Sugar Land, TX, 2006.
[3] H.F.W. Taylor, Cement Chemistry, 2nd ed, 1997 Telford, London.
[4] G.W. Scherer, G.P. Funkhouser, S. Peethamparan, Effect of pressure on early hydration of Class H cement, Cem. Concr. Res. 40 (2010) 845–850.
[5] L.J. Parrott, M. Geiker, W.A. Gutteridge, D. Killoh, Monitoring Portland cement hydration: comparison of methods, Cem. Concr. Res. 20 (6) (1990) 919–926.
[6] G. Sant, M. Dehadrai, D. Bentz, P. Lura, C.F. Ferraris, J.W. Bullard, J. Weiss, Detecting the fluid-to-solid transition in cement pastes, Comparing experimental and numerical techniques, Concrete International-A contribution from ACI Committee, vol. 236, 2009, pp. 53–58.
[7] J.W. Bullard, A determination of hydration mechanisms for tricalcium silicate using a kinetic cellular automaton model, J. Am. Ceram. Soc. 91 (7) (2008) 2088–2097.
[8] J.J. Thomas, A new approach to modeling the nucleation and growth kinetics of tricalcium silicate hydration, J. Am. Ceram. Soc. 90 (10) (2007) 3282–3288.
[9] D.P. Bentz, Three-dimensional computer simulation of cement hydration and microstructure development, J. Am. Ceram. Soc. 80 (1) (1997) 3–21.
[10] K. van Breugel, Modelling of cement-based systems — the alchemy of cement chemistry, Cem. Concr. Res. 34 (9) (2004) 1661–1668.
[11] S. Bishnoi, K.L. Scrivener, μic: a new platform for modelling the hydration of cements, Cem. Concr. Res. 39 (4) (2009) 266–274.
[12] A.C. Jupe, A.P. Wilkinson, K. Luke, G.P. Funkhouser, Class H oil well cement hydration at elevated temperatures in the presence of retarding agents: an in situ high-energy X-ray diffraction study, Ind. Eng. Chem. Res. 44 (15) (2005) 5579–5584.
[13] A.C. Jupe, A.P. Wilkinson, K. Luke, G.P. Funkhouser, Class H cement hydration at 180 °C and high pressure in the presence of added silica, Cem. Concr. Res. 38 (5) (2008) 660–666.
[14] M. Avrami, Kinetics of phase change. I General theory, J. Chem. Phys. 7 (1939) 1103–1112.
[15] M. Avrami, Kinetics of phase change. II Transformation-time relations for random distribution of nuclei, J. Chem. Phys. 8 (1940) 212–224.
[16] M. Avrami, Kinetics of phase change. III Granulation, phase change, and microstructure, J. Chem. Phys. 9 (1941) 177–184.
[17] J.W. Cahn, The kinetics of grain boundary nucleated reactions, ACTA Metall. 4 (1956) 449–459.
[18] J.W. Cahn, Transformation kinetics during continuous cooling, ACTA Metall. 4 (1956) 572–575.
[19] H.M. Jennings, J.J. Thomas, J.S. Gevrenov, G. Constantinides, F.-J. Ulm, A multi-technique investigation of the nanoporosity of cement paste, Cem. Concr. Res. 37 (3) (2007) 329–336.
[20] W.J. Caveny, R.L. Morgan, US Patent 7435293 — Cement compositions comprising maltodextrin, U.S. Patent, 2008.
[21] W.C. Frederick, US Patent 3132693—Composition comprising hydroxyethyl cellulose, polyvinylpyrrolidone and organic sulfonate, cement slurry prepared therefrom and method of cementing wells therewith, U.S. Patent, 1964.
[22] M. Sonebi, Rheological properties of grouts with viscosity modifying agents as diutan gum and welan gum incorporating pulverised fly ash, Cem. Concr. Res. 36 (9) (2006) 1609–1618.
[23] R. Helmuth, L.M. Hills, D.A. Whiting, S. Bhattacharja, Abnormal concrete performance in the presence of admixtures, Research & Development Information, Portland Cement Association (PCA), Skakie, Illinois, 1995.
[24] C.F. Ferraris, Measurement of the rheological properties of cement paste: a new approach, RILEM International Symposium, 1999, RILEM, Monterrey, Mexico.
[25] M. Geiker, Studies of Portland Cement Hydration by Measurements of Chemical Shrinkage and a Systematic Evaluation of Hydration Curves by Means of the Dispersion Model, in Institute of Mineral Industry, Technical University of Denmark, 1983.
[26] M. Geiker, T. Knudsen, Chemical shrinkage of Portland cement pastes, Cem. Concr. Res. 12 (5) (1982) 603–610.
[27] G. Sant, P. Lura, J. Weiss, Measurement of volume change in cementitious materials at early ages: review of testing protocols and interpretation of results, Transp. Res. Rec.: J. Transp. Res. Board (2007) 21–29 Issue 1979/2006.
[28] P. Mounanga, V. Baroghel-Bouny, A. Loukili, A. Khelidj, Autogenous deformations of cement pastes: part I. Temperature effects at early age and micro–macro correlations, Cem. Concr. Res. 36 (1) (2006) 110–122.
[29] S. Peethamparan, E. Weissinger, J. Vocaturo, J. Zhang, G. Scherer, Monitoring Chemical Shrinkage Using Pressure Sensors, ACI Special Proceedings in CD on ADVANCES in the Material Science of Concrete, 2010, pp. 77–88.
[30] C.M. Sayers, A. Dahlin, Propagation of ultrasound through hydrating cement pastes at early times, J. Adv. Cem. Based Mater. 1 (1) (1993) 12–21.
[31] J. Zhang, L. Qin, Z. Li, Hydration monitoring of cement-based materials with resistivity and ultrasonic methods, Mater. Struct. 42 (1) (2009) 1–10.
[32] H.W. Reinhardt, C.U. Grosse, Continuous monitoring of setting and hardening of mortar and concrete, Constr. Build. Mater. 18 (3) (2004) 145–154.
[33] J. Blitz, G. Simpson, Ultrasonic Methods of Non-destructive Testing, Chapman & Hall, London, 1996.
[34] G. Sant, C.F. Ferraris, J. Weiss, Rheological properties of cement pastes: a discussion of structure formation and mechanical property development, Cem. Concr. Res. 38 (11) (2008) 1286–1296.
[35] L.E. Copeland, J.C. Hayes, The determination of non-evaporable water in hardened Portland cement pastes, PCA Bull. 47 (1953).
[36] L. Molina, On predicting the influence of curing conditions on the degree of hydration, CBI Report 5:92, Swedish Cement and Concrete Research Institute, Stockholm, 1992.
[37] P. Mounanga, A. Khelidj, L. Ahmed, V. Baroghel-Bouny, Predicting $Ca(OH)_2$ content and chemical shrinkage of hydrating cement pastes using analytical approach, Cem. Concr. Res. 34 (2) (2004) 255–265.
[38] J. Zhang, G.W. Scherer, Comparison of quenching methods in cement, to be submitted to Cem. Concr. Res. (2010).
[39] E.M. Gartner, J.F. Young, D.A. Damidot, I. Javed, Hydration of Portland cement, in: J. Bensted, P. Barnes (Eds.), Structure and Performance of Cements, 2nd ed, Spon, London, 2002, pp. 57–108.
[40] F. Beltzung, F.H. Wittmann, Early chemical shrinkage due to dissolution and hydration of cement, Mater. Struct. 34 (5) (2001) 279–283.
[41] M.E. Chenevert, B.K. Shrestha, Chemical shrinkage properties of oilfield cements, SPE Drilling Eng. 6 (1) (1991) 37–43.
[42] H. Justnes, D. van Loo, B. Reyniers, P. Skalle, J. Sveen, E.J. Sellevold, Chemical shrinkage of oil well cement slurries, Adv. Cem. Res. 7 (26) (1995) 85–90.
[43] V. Baroghel-Bouny, P. Mounanga, A. Khelidj, A. Loukili, N. Rafai, Autogenous deformations of cement pastes: part II. W/C effects, micro–macro correlations, and threshold values, Cem. Concr. Res. 36 (1) (2006) 123–136.
[44] M. Bouasker, P. Mounanga, P. Turcry, A. Loukili, A. Khelidj, Chemical shrinkage of cement pastes and mortars at very early age: effect of limestone filler and granular inclusions, Cem. Concr. Compos. 30 (1) (2008) 13–22.
[45] H.M. Jennings, Aqueous solubility relationships for two types of calcium silicate hydrate, J. Am. Ceram. Soc. 69 (8) (1986) 614–618.
[46] D.D. Double, A. Hellawell, S.J. Perry, The hydration of Portland cement, Proc. R. Soc. Lond. A Math. Phys. 359 (1699) (1978) 435–451.
[47] S. Garrault, A. Nonat, Hydrated layer formation on tricalcium and dicalcium silicate surfaces: experimental study and numerical simulations, Langmuir 17 (26) (2001) 8131–8138.
[48] S. Garrault, T. Behr, A. Nonat, Formation of the C–S–H layer during early hydration of tricalcium silicate grains with different sizes, J. Phys. Chem. 110 (1) (2006) 270–275.
[49] T.C. Powers, T.L. Brownyard, Studies on the Physical Properties of Hardened Portland Cement Paste, PCA Bulletin 22, Vol. III, Portland Cement Association, Chicago, 1948.
[50] K.O. Kjellsen, R.J. Detwiler, O.E. Gjorv, Backscattered electron imaging of cement pastes hydrated at different temperatures, Cem. Concr. Res. 20 (2) (1990) 308–311.
[51] K.O. Kjellsen, R.J. Detwiler, O.E. Gjorv, Development of microstructures in plain cement pastes hydrated at different temperatures, Cem. Concr. Res. 21 (1) (1991) 179–189.
[52] K.O. Kjellsen, R.J. Detwiler, Reaction kinetics of Portland cement mortars hydratedat different temperatures, Cem. Concr. Res. 22 (1) (1992) 112–120.
[53] J.I. Escalante-Garcia, Nonevaporable water from neat OPC and replacement materials in composite cements hydrated at different temperatures, Cem. Concr. Res. 33 (11) (2003) 1883–1888.
[54] H.M. Jennings, A model for the microstructure of calcium silicate hydrate in cement paste, Cem. Concr. Res. 30 (1) (2000) 101–116.
[55] A. Bentur, R.L. Berger, J.H. Kung, N.B. Milestone, J.F. Young, Structural properties of calcium silicate pastes: II, effect of the curing temperature, J. Am. Ceram. Soc. 62 (7–8) (1979) 362–366.
[56] F. Lin, C. Meyer, Hydration kinetics modeling of Portland cement considering the effects of curing temperature and applied pressure, Cem. Concr. Res. 39 (4) (2009) 255–265.
[57] J.J. Thomas, H.M. Jennings, A.J. Allen, Relationships between composition and density 921 of tobermorite, jennite, and nanoscale $CaO–SiO_2–H_2O$, J. Phys. Chem. C in press.
[58] P. Acker, Swelling, shrinkage and creep: a mechanical approach to cement hydration, Mater. Struct. 37 (2004) 237–243.
[59] D.P. Bentz, P.V. Coveney, E.J. Garboczi, M.F. Kleyn, P.E. Stutzman, Cellular automaton simulations of cement hydration and microstructure development, Modell. Simul. Mater. Sci. Eng. 2 (4) (1994) 783–808.
[60] C.M. Sayers, R.L. Grenfell, Ultrasonic propagation through hydrating cements, Ultrasonics 31 (3) (1993) 147–153.
[61] J.J. Thomas, H.M. Jennings, Effect of heat treatment on the pore structure and drying shrinkage behavior of hydrated cement paste, J. Am. Ceram. Soc. 85 (9) (2002) 2293–2298.
[62] I. Elkhadiri, M. Palacios, F. Puertas, Effect of curing temperature on cement hydration, Ceramics-Silikáty 53 (2) (2009) 65–75.
[63] J.J. Thomas, A.J. Allen, H.M. Jennings, Hydration kinetics and microstructure development of normal and $CaCl_2$-accelerated tricalcium silicate pastes, J. Phys. Chem. C 113 (46) (2009) 19836–19844.